



1 Comparing observed and modelled components of the Atlantic Meridional Overturning  
2 Circulation at 26°N.

3  
4 Harry Bryden<sup>1</sup>, Sybren Drijfhout<sup>1,2</sup>, Jennifer Mecking<sup>3</sup>, Wilco Hazeleger<sup>2</sup>

5  
6 <sup>1</sup>Ocean and Earth Science, University of Southampton, Southampton United Kingdom

7 <sup>2</sup>Faculty of Geosciences, University of Utrecht, Utrecht, The Netherlands

8 <sup>3</sup>National Oceanography Centre, Southampton, United Kingdom

9  
10 Correspondence Email: [hlb@soton.ac.uk](mailto:hlb@soton.ac.uk)

11  
12 15 November 2023

### 13 14 **Abstract**

15  
16 The Coupled Model Intercomparison Project (CMIP) allows assessment of the representation  
17 of the Atlantic Meridional Overturning Circulation (AMOC) in climate models. While CMIP  
18 Phase 6 models display a large spread in AMOC strength by a factor of three, the multi-model  
19 mean strength agrees reasonably well with observed estimates from RAPID<sup>1</sup>, but this does not  
20 hold for its various components. In CMIP6 the present-day AMOC is characterised by a lack  
21 of lower North Atlantic Deep Water (INADW), due to the small-scale of Greenland-Iceland-  
22 Scotland Ridge overflow and too much mixing. This is compensated by increased  
23 recirculation in the subtropical gyre and more Antarctic Bottom Water (AABW). Deep-water  
24 circulation is dominated by a distinct deep western boundary current (DWBC) with minor  
25 interior recirculation compared to observations. The future decline in the AMOC to 2100 of  
26 7Sv under a SSP5-8.5 scenario is associated with decreased northward western boundary  
27 current transport in combination with reduced southward flow of upper North Atlantic Deep  
28 Water (uNADW). In CMIP6, wind stress curl decreases with time by 14% so that the wind-  
29 driven thermocline recirculation in the subtropical gyre is reduced by 4 Sv (17%) by 2100.  
30 The reduction in western boundary current transport of 11Sv is more than the decrease in the  
31 wind-driven gyre transport suggesting a decrease over time in the component of the Gulf  
32 Stream originating in the South Atlantic.

### 33 34 **1. Introduction**

35  
36 The Atlantic Meridional Overturning Circulation (AMOC) is the Atlantic part of the global  
37 overturning circulation. Our understanding of the strength, variability and structure of the  
38 AMOC has improved since the deployment of the RAPID<sup>1</sup> array, which monitors the volume  
39 transport at 26°N since April 2004 (Moat et al., 2020). Additionally, these observations serve  
40 as invaluable reference data for the representation of the AMOC in coupled climate and Earth  
41 System models. The most recent phase of the Coupled Model Intercomparison Project, CMIP  
42 Phase 6, allows us to assess the representation of the AMOC in these models. The models  
43 project the AMOC strength will decline over the next century (Lee et al., 2021). Here we  
44 compare observed and modeled components of the AMOC over the historical period 2004 to  
45 2014 and then assess how the ensemble-mean CMIP6 transport components change in a  
46 declining AMOC over the next century under SSP5-8.5 emission scenario.

---

<sup>1</sup> RAPID is used here as shorthand for the RAPID-Meridional Overturning Circulation and Heatflux Array-Western Boundary Time Series at 26°N (Moat et al., 2022).



47

48 The RAPID AMOC observations from 2004 to 2018 indicate that the AMOC has declined by  
49 2.4 Sv, about 12%, from 18.3 Sv to 15.9 Sv (Bryden, 2021). The decline is primarily evident  
50 in reduced southward transport of lower North Atlantic Deep Water (LNADW) that is  
51 balanced by slightly reduced Gulf Stream transport and more southward recirculation within  
52 the subtropical gyre. In CMIP6 models, the AMOC declines by about 40% over the 21st  
53 century (Weijer et al., 2020). Here we analyse 19 CMIP6 model projections in order to  
54 identify which components lead to the AMOC decline, for clues as to how the AMOC may  
55 change within the continuing RAPID observational framework.

56

57 The Coupled Model Intercomparison Project (CMIP) is a comprehensive effort of modelling  
58 centres around the world to improve our understanding about past, present and future changes  
59 of the climate system (Eyring et al., 2016; O'Neill et al., 2016). Even though CMIP6 shows  
60 improvements compared to previous CMIP generations, model biases related to the AMOC  
61 persist. These include a shallow bias to the deep cell, too much deep convection, and a too-  
62 small temperature difference between its upper and lower limbs. Additionally, CMIP6  
63 models largely underestimate low-frequency variability of the AMOC and show large inter-  
64 model differences in their AMOC representation (Weijer et al., 2020).

65

66 The RAPID array monitors the AMOC volume transport at 26°N since April 2004 (Smeed et  
67 al., 2018). The transport through the cross section is estimated by a decomposition of the  
68 AMOC into 3 components: (1) transport through the Florida Straits, (2) Ekman surface  
69 transport generated by zonal wind stress, and (3) density driven interior transport estimated  
70 from mooring measurements. The mid-ocean interior transport is further broken down into  
71 thermocline recirculation (0-800m depth), intermediate water transport (800-1100m), upper  
72 North Atlantic Deep Water (1100-3000m), lower North Atlantic Deep Water (3000-5000m).  
73 The goal of this study is to gain insight into the cause of disagreement between CMIP6  
74 models and RAPID data in terms of AMOC strength, structure and variability. We  
75 decompose the modelled AMOC transport at 26°N from CMIP6 into the same transport  
76 components as measured by the RAPID array. We compare the CMIP6 transport components  
77 with the observed Rapid components for the historical period 2004-2014. We then examine  
78 the change of these components in CMIP6 under the SSP5-8.5 emission scenario from the  
79 historical period until 2100.

80

## 81 **2. Data and Methods**

82

83 Monthly averages of AMOC estimates from the RAPID array are compared to the historical  
84 simulations of 19 CMIP6 models. Note that only the overlapping period was investigated,  
85 April 2004 – December 2014. Details of the 19 CMIP6 models are given in Table 1. The  
86 SSP5-8.5 future projection from 2015 to 2100, is then used to investigate how the AMOC  
87 may change in future projections. For each model, one ensemble member was used.

88



Table 1: Metadata and references of the models analysed in this study. References are from the Earth System Grid Federation

Model	Modelling centre	Horizontal resolution (°)	Variant label	Data reference historical	Data reference SSP585
CAMS-CSM1-0	CAMS	1 x 1	r1i1p1f1	Rong (2019)	Rong (2019)
CAS-ESM2-0	CAS	1 x 1	r1i1p1f1	Chai (2020)	Unknown (2018)
CESM2-WACCM	NCAR	1 x 1	r1i1p1f1	Danabasoglu (2019)	Danabasoglu (2019)
CIESM	THU	1 x 1	r1i1p1f1	Huang (2019)	Huang (2020)
CMCC-CM2-SR5	CMCC	1 x 1	r1i1p1f1	Lovato and Peano (2020)	Lovato and Peano (2020)
CMCC-ESM2	CMCC	1 x 1	r1i1p1f1	Lovato et al. (2021)	Lovato et al. (2021)
CNRM-CM6-1	CNRM-CERFACS	1 x 1	r1i1p1f2	Voltaire (2019)	Voltaire (2019)
CNRM-ESM2-1	CNRM-CERFACS	1 x 1	r2i1p1f2	Seferian (2018)	-
CanESM5	CCCma	1 x 1	r1i1p1f1	Swart et al. (2019)	Swart et al. (2019)
EC-Earth3	EC-Earth Consortium	1 x 1	r1i1p1f1	EC-Earth Consortium (2021)	EC-Earth Consortium (2019)
FIO-ESM-2-0	FIO-QLNM	1 x 1	r1i1p1f1	Song et al. (2019)	Song et al. (2019)
HadGEM3-GC31-LL	MOHC	1 x 1	r1i1p1f3	Ridley et al. (2019)	Good (2020)
HadGEM3-GC31-MM	MOHC	0.25 x 0.25	r1i1p1f3	Ridley et al. (2019)	Ridley et al. (2019)
IPSL-CM6A-LR	IPSL	1 x 1	r1i1p1f1	Boucher et al. (2021)	Boucher et al. (2019)
MPI-ESM1-2-HR	MPI	0.4 x 0.4	r1i1p1f1	Jungclaus et al. (2019)	Schupfner et al. (2019)
MPI-ESM1-2-LR	MPI	1.5 x 1.5	r1i1p1f1	Wieners et al. (2019)	Wieners et al. (2019)
MRI-ESM2-0	MRI	1 x 0.5	r1i1p1f1	Yukimoto et al. (2019)	Yukimoto et al. (2019)
NESM3	NUIST	1 x 1	r1i1p1f1	Cao and Wang (2019)	Cao (2019)
UKESM1-0-LL	MOHC	1 x 1	r1i1p1f2	Tang et al. (2019)	Good et al. (2019)

89

90 A cross section between Florida and the African continent at the latitude closest to 26°N was  
 91 selected for each model. The net transport through the section, approximately -1 Sv for each  
 92 model due to the Bering Strait throughflow, was removed before computing the AMOC  
 93 components from meridional velocities as follows:

94

95 Florida Straits Transport (FS): CMIP6 models do not resolve the Bahama Islands and as a  
 96 result the Florida Straits proper. For this reason the following definition is used. The  
 97 boundary between Florida Straits (FS) transport and mid-ocean transport is defined as the  
 98 longitude where the depth-averaged transport (from the surface down to the depth of  
 99 maximum overturning) changes from positive (northward) to negative (southward). This  
 100 definition thus identifies the FS transport as the western boundary current, thereby including  
 101 the transport by the Antilles Current, which in CMIP6 models cannot be separated from the  
 102 Florida Current.

103

104 Thermocline Recirculation (tr): East of FS and from the surface to down to the depth of  
 105 horizontally averaged potential temperature of 8°C.

106

107 Intermediate Waters (iw): East of FS and between the depth of horizontally averaged potential  
 108 temperature of 8°C and depth of maximum overturning.

109

110 Upper North Atlantic Deep Water (uNADW): Between the depth of maximum overturning  
 111 and the depth of horizontally averaged potential temperature of 3°C.

112

113 Lower North Atlantic Deep Water (lNADW): Between the depth of horizontally averaged  
 114 potential temperature of 3°C and the depth where horizontally-averaged transport changes  
 115 from negative to positive.

116

117 Antarctic Bottom Water (AABW): Between the depth where horizontally-averaged transport  
 118 changes from negative to positive and the bottom.



119

120 Ekman (ek): Near surface ageostrophic transport estimated from the zonal wind stress.

121

122 Multi-model means (MMM) for each component over the 19 models are then made with their  
123 standard deviation.

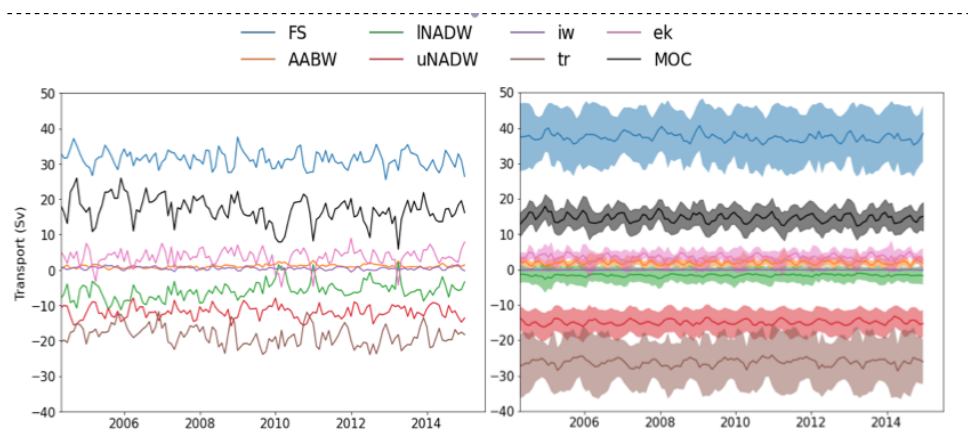
124

### 125 3. Results

126

127 Figure 1 compares the RAPID observations of the AMOC transport components with the  
128 CMIP6 components for the historical period 2004-2014. For the historical period (2004-  
129 2014) the MMM CMIP6 AMOC underestimates the observed AMOC transport by 2.2 Sv  
130 (Table 2). The underestimation of AMOC strength in the CMIP6 models is likely related to  
131 the reduced transport of lower NADW, due to the small scale of Greenland-Iceland-Scotland  
132 Ridge overflow compared to the resolution of models and excessive mixing at this location. In  
133 a study of deep waters in CMIP6, Heuzé (2021) noted that the models did form water masses  
134 similar in properties to INADW in the Nordic Seas, but none of the deep waters made it over  
135 the ridge and into the Iceland or Irminger basins. In the models, this lack of INADW is  
136 partially compensated by increased southward flow of upper NADW so the total southward  
137 flow of deep water in CMIP6 is comparable to that observed by RAPID. The variability of  
138 NADW is underestimated, most likely due to the inability of models to reproduce lower  
139 NADW overflow. Deep-water circulation in models is dominated by a distinct DWBC with  
140 minor interior recirculation compared with observations. CMIP6 MMM Florida Straits (FS)  
141 transport (37.4 Sv) is larger than observed Florida Straits transport (31.3 Sv). The relatively  
142 coarse-resolution models do not resolve the narrow Florida Straits, and the model western  
143 boundary current includes the narrow Antilles Current east of the Bahamas as well as the Gulf  
144 Stream flow through Florida Straits. Recent estimates of Antilles Current transport are about  
145 5 Sv (Meinen et al., 2019) and adding this transport to the observed Florida Straits transport  
146 suggests that the observed (36.3 Sv) and modeled (37.4 Sv) western boundary current  
147 transports are similar. The low-frequency variability of Florida Straits transport is largely  
148 overestimated in CMIP6 models and we hypothesize that the inclusion of the Antilles Current  
149 in this component in models may be a significant contributor to this variability as the  
150 observed Antilles Current transport exhibits rms variability of 10 Sv that is not correlated  
151 with Florida Straits transport variability. The MMM thermocline recirculation (tr) in CMIP6  
152 models (-26.2 Sv) is larger than observed by the RAPID array (-18.6 Sv) though again this  
153 may be due to issues on how the Antilles Current transport is accounted in the observations  
154 and in the models. RAPID estimates thermocline recirculation to be the overall southward  
155 flow between the Bahamas and Africa and this overall flow includes both the Antilles Current  
156 transport and the mid-ocean thermocline recirculation associated with the wind-driven  
157 subtropical gyre. If we separate out the northward Antilles Current transport of 5 Sv, then the  
158 mid-ocean thermocline recirculation for RAPID would be -23.6 Sv (Table 2) in more  
159 reasonable agreement with the CMIP6 MMM thermocline circulation of -26.2 Sv. Overall,  
160 the MMM circulation in CMIP6 models for the historical period reasonably represents the  
161 observed circulation in RAPID except for the underestimated INADW transport associated  
162 with issues of model representation of flows over ridges.

163



164  
 165 Figure 1. Historical time series for RAPID data (left) and multi-model mean CMIP6 data  
 166 (right). Shaded areas indicate one standard deviation of the ensemble spread. This is Figure 6  
 167 in Beunk (2022)  
 168

Table 2. Components of the Atlantic Meridional Overturning Circulation at 26°N

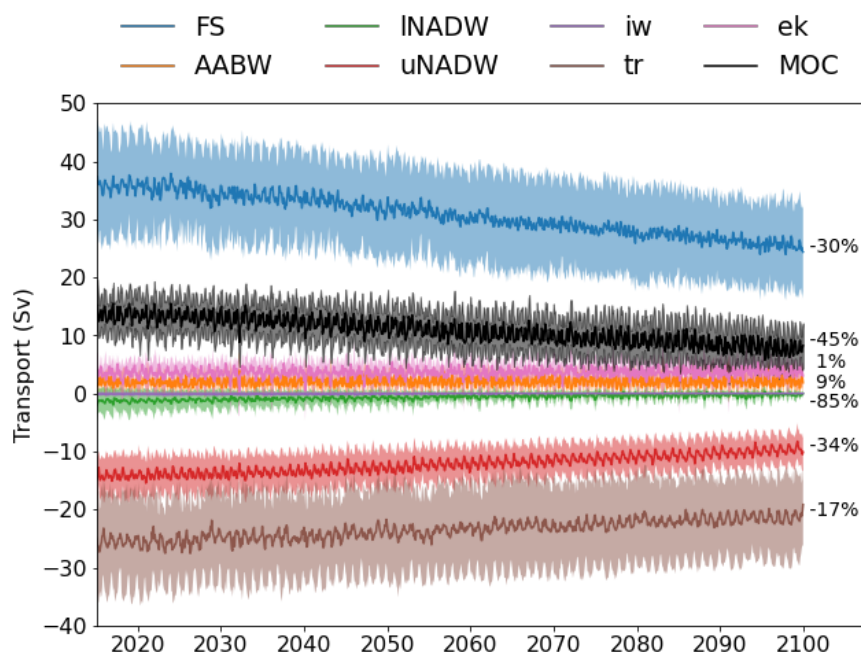
	Rapid (2004-14)	CMIP6 Average		Decline
		Historical (2004-14)	2090-2100	
<b>Upper Water</b>				
Florida Straits (FS)	31.3			
Ekman	3.6	3.5	3.4	0.1 (1%)
Intermediate Water (IW)	0.4	---	---	
Thermocline Recirculation (TR)	-18.6			
AMOC=FS+Ekman+IW+TR	16.7			
<b>Antilles Current (AC)</b>				
Antilles Current (AC)	5			
Western Boundary Current (FS+AC)	36.3	37.4	26.4	11 (30%)
Thermocline Recirculation +AC	-23.6			
Model Thermocline Recirculation		-26.2	-21.8	4.4 (17%)
Western Boundary Current+Ekman+Model TR		14.7	8.0	6.7 (45%)
<b>Deep Water</b>				
uNADW	-11.9	-14.9	-9.9	5.0 (34%)
INADW	-5.9	-1.6	-0.2	1.4 (85%)
AABW	1.0	1.9	2.1	-0.2 (9%)
AMOC=uNADW+INADW+AABW	-16.8	-14.6	-8.0	6.6 (45%)

169  
 170 CMIP6 model projections suggest that the AMOC will decline over the next century as noted  
 171 by Weijer et al. (2020). Here we find that the AMOC declines by 45% over the period 2015  
 172 to 2100 in a MMM of 19 CMIP6 projections. For comparison, over the RAPID time period  
 173 2004 to 2021, the AMOC has exhibited a small (order 12%) reduction that is manifest  
 174 principally in reduced southward transport of INADW (Bryden, 2021). It is of interest to  
 175 identify which components contribute to the projected 45% decline in the AMOC over the  
 176 coming century in CMIP6 simulations.

177  
 178 All 19 CMIP6 models analysed here exhibit a decline in the AMOC over the 21st century



179 (Table 3). This decline of the AMOC under SSP5-8.5 is in line with other modelling studies  
180 (Levang and Schmitt, 2020; Weijer et al, 2020; Roberts et al., 2020). Averaged over the 19  
181 models, the AMOC decline from 2004-2014 to 2090-2100 is 6.6 Sv or 45% in the AMOC  
182 transport for the historical period (Figure 2). We find that the decline in the AMOC at 26°N  
183 in CMIP6 models from 2015 to 2100 is dominated by a 30% decrease in western boundary  
184 current transport (FS in Figure 2) and a 34% reduction in southward deep water transport  
185 (uNADW in Figure 2). As Ekman transport (ek) shows no significant change in the model  
186 projections, the AMOC decline of 6.6 Sv in the upper waters is the result of the difference  
187 between the decline in western boundary current (FS) transport of 11.0 Sv and the 17%  
188 decline in southward thermocline recirculation (tr) of 4.4 Sv. For the lower waters the overall  
189 decline in northward transport of upper waters of 6.6 Sv is compensated by a decrease in  
190 uNADW transport of 6.4 Sv and a small increase in northward AABW transport of 0.2 Sv, so  
191 that the net transport through the cross section remains zero.  
192



193  
194 Figure 2. Multi-model mean timeseries of each component under SSP5-8.55. Shaded areas  
195 illustrate one standard deviation of the inter-model spread. Percentages show the decline  
196 relative to the historical period. This is Figure 12 In Beunk (2022).  
197



<i>Model name</i>	<i>Historical mean (Sv)</i>	<i>2090-2100 mean (Sv)</i>	<i>Change (Sv)</i>	<i>Change (%)</i>
<i>CAMS-CSM1-0</i>	12.4	8.9	-3.5	-28
<i>CAS-ESM2-0</i>	18.4	13.7	-4.7	-26
<i>CESM2-WACCM</i>	17.9	6.8	-11.1	-62
<i>CIESM</i>	11.4	4	-7.4	-65
<i>CMCC-CM2-SR5</i>	14.2	9.2	-5.0	-35
<i>CMCC-ESM2</i>	13.3	9.3	-4.0	-30
<i>CNRM-CM6-1</i>	15.7	6.9	-8.8	-56
<i>CNRM-ESM2-1</i>	15.3			
<i>CanESM5</i>	11.4	5.5	-5.9	-52
<i>EC-Earth3</i>	16.2	10.7	-5.5	-34
<i>FIO-ESM-2-0</i>	17.7	10.7	-7.0	-39
<i>HadGEM3-GC31-LL</i>	15.2	7.9	-7.3	-48
<i>HadGEM3-GC31-MM</i>	15.4	6.5	-8.9	-58
<i>IPSL-CM6A-LR</i>	11.6	6.5	-5.1	-44
<i>MPI-ESM1-2-HR</i>	14.8	8.6	-6.2	-42
<i>MPI-ESM1-2-LR</i>	16.6	11.4	-5.2	-31
<i>MRI-ESM2-0</i>	15.4	5	-10.4	-67
<i>NESM3</i>	9.0	5	-4.0	-45
<i>UKESM1-0-LL</i>	15.6	7.8	-7.8	-50

198  
 199 Table 3. Values of the total AMOC for every model. Shown are the historical mean values,  
 200 2090-2100 mean values, absolute change and relative change. Changes are relative to the  
 201 historical period. This Table is Appendix G in Beunk (2022).

202  
 203 To examine changes in wind-driven circulation over the 21<sup>st</sup> century in the subtropical North  
 204 Atlantic, we examined the mean wind-stress curl along the 26°N section for the historical and  
 205 SSP585 period. The values are negative (i.e. clockwise rotation), which results in southward  
 206 mid-ocean Sverdrup transport. Since the upper level gyre circulation is driven by wind-stress  
 207 curl (DiNezio et al., 2009; Zhao and Johns, 2014), we expect a decrease of this driver to affect  
 208 both Florida Straits transport and thermocline recirculation. Averaged over the model  
 209 projections, wind stress curl decreases by 14% from about  $6 \times 10^{-8} \text{ m s}^{-2}$ . On the basis of  
 210 Sverdrup dynamics, we expect this change in wind stress curl will reduce the thermocline  
 211 recirculation at 26°N and indeed the thermocline recirculation does decrease by 4.4 Sv or  
 212 17% over the 21<sup>st</sup> century. We conclude that the reduction of thermocline recirculation is  
 213 almost entirely caused by a decline in wind-stress curl. On the basis of western  
 214 intensification theory (Stommel, 1948), the decrease in wind-stress curl should also lead to a  
 215 decrease in western boundary current transport by a similar amount. Thus we can explain a  
 216 decrease in western boundary current transport of 4.4 Sv over the 21st century as being due to  
 217 changes in the wind forcing.

218  
 219 The change in the western boundary current transport of 11 Sv in the CMIP projections is due  
 220 to a reduction in the wind-driven component by 4.4 Sv and to a reduction in the component of  
 221 the Gulf Stream flow originating from the South Atlantic of 6.6 Sv. The overall 6.6 Sv  
 222 reduction in the northward flow in the upper waters is then compensated by a reduction in  
 223 southward flow of the deep waters. In CMIP6, the reduction in the southward flow of deep  
 224 water is almost entirely due to a decreased DWBC transport of uNADW over the period  
 225 2015-2100. Thus the projected AMOC reduction over the 21st century in CMIP6 is due to a  
 226 reduction in the thermohaline circulation where there is less northward transport of upper  
 227 waters principally in the western boundary current across 26°N and less southward deep water  
 228 transport in the deep western boundary current.

229  
 230



#### 231 **4. Discussion**

232

233 Over the SSP5-8.5 period (2015-2100) in CMIP6 projections, we find declines in the western  
234 boundary current transport, thermocline recirculation and NADW transport. Decreased  
235 thermocline recirculation is related to a decline in wind stress curl along the section and this  
236 decline is also expected to contribute to the decline in Gulf Stream transport. But the decline  
237 in western boundary current transport in CMIP6 models is substantially greater than the  
238 decline in wind stress curl and accompanying thermocline recirculation. Therefore, for the  
239 upper water circulation the CMIP6 decline in the AMOC is mostly caused by a decrease in  
240 the component of the western boundary current associated with the thermohaline circulation.  
241 For the lower water circulation, the decline in southward transport over the SSP5-8.5 period is  
242 associated with reduced uNADW transport. The overall reduction in southward deep water  
243 transport suggests a decline in NADW formation.

244

245 In a similar study, Asbjornsen and Arthun (2023) examined future changes in the AMOC  
246 using 14 CMIP6 models and found a weakening AMOC by 8.5 Sv over the coming century.  
247 For their ensemble, the Gulf Stream weakened by 33% or 11.2 Sv, 3.7 Sv of which was due to  
248 change in wind stress, and the Deep Western Boundary Current transport weakened by 8.5  
249 Sv. As noted above, the CMIP6 projections are consistent in projecting a decline in the  
250 AMOC this century (Table 3), but the exact size of the AMOC reduction depends on which  
251 models are used for the study.

252

253 Because the AMOC is responsible for most of the northward heat transport in the Atlantic  
254 Ocean (Johns et al., 2011; Johns et al., 2023), CMIP6 model projections also exhibit a  
255 decrease in northward heat transport at 26°N over the 2015-2100 time period (Mecking and  
256 Drijfhout, 2023). The northward ocean heat transport across 26°N decreases by an average of  
257 0.3 PW for the SSP5-8.5 scenario and this represents a 30% decline from the historical value  
258 of 1.0 PW.

259

260 The decline in the thermohaline circulation at 26°N implies that the overturning circulation  
261 south of 26°N, that is in the global circulation outside the North Atlantic, has also changed.  
262 The extra-Atlantic circulation converts deep water into upper and intermediate waters so that  
263 the southward deep water flow across 26°N and out of the North Atlantic must ultimately be  
264 converted within the global ocean into upper and intermediate waters that flow back into the  
265 North Atlantic and northward across 26°N. The decline in the North Atlantic thermohaline  
266 circulation at 26°N suggests that this global-scale overturning circulation must also have  
267 changed. Baker et al (2023) have explored how 2 mechanisms converting deep water into  
268 upper water south of 26°N change within CMIP6 simulations. The 2 mechanisms considered  
269 are Southern Ocean upwelling associated with eastward wind stress around Antarctica  
270 (Toggweiler and Samuels, 1993) and Indo-Pacific diffusive upwelling associated with deep  
271 interior mixing (Munk, 1966). Baker et al. found that the wind stress around Antarctica did  
272 not decline enough to account for a reduced 6 Sv upwelling of deep water, in fact there  
273 appeared to be a small increase in Southern Ocean wind stress and upwelling. Instead they  
274 found evidence in the CMIP6 projections that the interior Indo-Pacific upwelling declined  
275 enough to account for reduced conversion of deep waters into thermocline waters. They  
276 attributed such decline to the global warming that increases stratification (Li et al., 2020) and  
277 inhibits vertical mixing and associated upwelling.

278

279 Overall, the Atlantic and global overturning circulations appear to have declined in CMIP6  
280 projections from 2015 to 2100. The manifestation of these declines at 26°N include a





281 reduction in the southward transport of NADW and a compensating reduction in the  
282 northward flow of upper and thermocline waters through Florida Straits. The reduction in  
283 southward deep water transport in CMIP6 is linked to a lack of INADW formed in the Nordic  
284 Seas flowing out over the Greenland-Iceland-Scotland Ridge into the northern Atlantic  
285 (Heuzé, 2021); and the reduction in northward flow of upper waters is linked to a decrease in  
286 diffusive upwelling in the Indo-Pacific related to increased stratification due to global  
287 warming (Li et al., 2020; Baker et al., 2023). The ability of coupled climate models to  
288 realistically include these critical processes of deep water formation, mixing in ridge  
289 overflows and mid-ocean diffusive upwelling for future projections of ocean circulation  
290 should be carefully assessed. In particular, the representation of deep water formation  
291 in coupled climate models could be examined in comparison with observed production of  
292 deep water. Implementing mixing parameterisations for overflows (Holt et al., 2017) in  
293 coupled climate models could be assessed for their effectiveness in allowing the southward  
294 transport of INADW into and through the North Atlantic. And coupled climate models could  
295 be examined for their parameterisations of diffusive mixing and upwelling, testing how  
296 different parameterisations affect the global ocean overturning circulation over century time  
297 scales.

298  
299 In terms of observations, our results suggest that the ongoing RAPID project should  
300 separately measure the Antilles Current and add it to Florida Straits transport for a true  
301 measure of western boundary current transport for comparison with modelled transport  
302 components. And the Antilles Current transport should be separated from the net mid-ocean  
303 southward flow across 26N in the upper 800m that RAPID labels thermocline recirculation so  
304 as to identify the actual mid-ocean thermocline recirculation associated with the wind stress  
305 curl. By separately estimating the Antilles Current transport contribution, the RAPID project  
306 could then provide well-defined estimates for the wind-driven and thermohaline contributions  
307 to the AMOC at 26°N.

308

### 309 **Code Availability**

310

311 The code used to obtain the results of this study and a file containing metadata of the models  
312 is freely available on GitHub: [https://github.com/jordibeunk/MSc\\_Thesis.git](https://github.com/jordibeunk/MSc_Thesis.git)

313

### 314 **Data Availability**

315 RAPID data and notes are freely available at

316 [https://rapid.ac.uk/rapidmoc/rapid\\_data/datadl.php](https://rapid.ac.uk/rapidmoc/rapid_data/datadl.php)

317 19 CMIP6 models are used. The choice of these models is motivated by the fact that both  
318 historical (2004-20015) data and future (2015-2100) projections under Shared Socioeconomic  
319 Pathway 5-8.5 are available for all used variables. The model data has been accessed through  
320 the Centre for Environmental Data Analysis (CEDA) archive <https://data.ceda.ac.uk>

### 321 **Author Contributions**

322

323 This work is based on an MSc thesis by Jordi Beunk at Utrecht University. Jennifer Mecking,  
324 Sybren Drijfhout and Harry Bryden designed the project. Sybren Drijfhout and Wilco  
325 Hazeleger identified the student and supervised the project in Utrecht while Mecking and  
326 Bryden provided advice during the project and write-up of the thesis. After finishing the  
327 thesis, Jordi Beunk indicated that he did not wish to be involved in writing up the results for



328 publication. Harry Bryden prepared a draft for this paper based on Beunk's thesis. Drijfhout,  
329 Mecking and Hazeleger then edited the draft and all authors added elements of discussion  
330 related to recent papers based on CMIP6 results.

331

### 332 **Competing interests**

333

334 The contact author declares that none of the authors has any competing interests

335

### 336 **Acknowledgments**

337 Bryden was a lead investigator for the NERC-funded project that first deployed the  
338 transocean Rapid instrument array in 2004 under grant NER/T/S/2002/00481 and he has  
339 continued to carry out analyses involving the ongoing Rapid observations following formal  
340 retirement in 2011. Drijfhout and Mecking have been funded by NERC under the Wider  
341 Impacts of Subpolar North Atlantic decadal variability on the ocean and atmosphere  
342 (WISHBONE) grant NE/T0133478/1.

343

### 344 **References**

345

346 Asbjørnsen, H. and Årthun, M., 2023. Deconstructing future AMOC decline at 26.5 N. *Geophysical*  
347 *Research Letters*, 50(14), p.e2023GL103515

348

349 Baker, J. S., Bell, M. J., Jackson, L. C., Renshaw, R., Vallis, G. K., Watson, A. J. & Wood, R. A. (2023).  
350 Overturning pathways control AMOC weakening in CMIP6 Models. *Geophysical Research Letters*, 50,  
351 e2023GL.103381.

352 <https://doi.org/10.1029/2023GL.103381>

353

354 Beunk, Jordi (2022). Comparing observed and modeled decomposition of the Atlantic Meridional  
355 Overturning Circulation at 26°N. MSc Thesis, Department of Geosciences, Utrecht University, 54p.

356

357 Boucher, Olivier; Denvil, Sébastien; Levvasseur, Guillaume; Cozic, Anne; Caubel, Arnaud; Foujols,  
358 Marie-Alice; Meurdesoif, Yann; Balkanski, Yves; Checa-Garcia, Ramiro; Hauglustaine, Didier; Bekki,  
359 Slimane; Marchand, Marion (2021). IPSL IPSL-CM6A-LR-INCA model output prepared for CMIP6 CMIP  
360 historical. Version 20211003. Earth System Grid Federation.

361 <https://doi.org/10.22033/ESGF/CMIP6.13601>

362

363 Boucher, Olivier; Denvil, Sébastien; Levvasseur, Guillaume; Cozic, Anne; Caubel, Arnaud; Foujols,  
364 Marie-Alice; Meurdesoif, Yann; Cadule, Patricia; Devilliers, Marion; Dupont, Elliott; Lurton,  
365 Thibaut (2019). IPSL IPSL-CM6A-LR model output prepared for CMIP6 ScenarioMIP ssp585.  
366 Version 20211003. Earth System Grid Federation. <https://doi.org/10.22033/ESGF/CMIP6.5271>

367

368 Bryden, H. L. (2021). Wind-driven and buoyancy-driven circulation in the subtropical North Atlantic  
369 Ocean. *Proceedings of the Royal Society A*, 477(2256), 20210172.

370

371 Buckley, M. W., & Marshall, J. (2016). Observations, inferences, and mechanisms of the Atlantic  
372 Meridional Overturning Circulation: A review. *Reviews of Geophysics*, 54(1), 5-63.

373

374 Cao, Jian (2019). NUIST NESMv3 model output prepared for CMIP6 ScenarioMIP ssp585.

375 Version 20211003. Earth System Grid Federation. <https://doi.org/10.22033/ESGF/CMIP6.8790>

376



- 377 Cao, Jian; Wang, Bin (2019). NUIST NESMv3 model output prepared for CMIP6 CMIP  
378 historical. Version 20211003.Earth System Grid Federation.  
379 <https://doi.org/10.22033/ESGF/CMIP6.8769>  
380
- 381 Chai, Zhaoyang (2020). CAS CAS-ESM1.0 model output prepared for CMIP6 CMIP historical.  
382 Version 20211003.Earth System Grid Federation. <https://doi.org/10.22033/ESGF/CMIP6.3353>  
383
- 384 Unkown (2018). CAS CAS-ESM1.0 model output prepared for CMIP6 ScenarioMIP ssp585. Earth  
385 System Grid Federation. [http://cera-www.dkrz.de/WDCC/meta/CMIP6/CMIP6.ScenarioMIP.CAS.CAS-](http://cera-www.dkrz.de/WDCC/meta/CMIP6/CMIP6.ScenarioMIP.CAS.CAS-ESM2-0.ssp585)  
386 [ESM2-0.ssp585](http://cera-www.dkrz.de/WDCC/meta/CMIP6/CMIP6.ScenarioMIP.CAS.CAS-ESM2-0.ssp585)  
387
- 388 Danabasoglu, Gokhan (2019). NCAR CESM2-WACCM model output prepared for CMIP6 ScenarioMIP  
389 ssp585. Version 20211003.Earth System Grid Federation.  
390 <https://doi.org/10.22033/ESGF/CMIP6.10115>  
391
- 392 Danabasoglu, Gokhan (2019). NCAR CESM2-WACCM-FV2 model output prepared for CMIP6 CMIP  
393 historical. Version 20211003.Earth System Grid Federation.  
394 <https://doi.org/10.22033/ESGF/CMIP6.11298>  
395
- 396 DiNezio, P. N., Gramer, L. J., Johns, W. E., Meinen, C. S., & Baringer, M. O. (2009). Observed  
397 interannual variability of the Florida Current: Wind forcing and the North Atlantic Oscillation. *Journal*  
398 *of Physical Oceanography*, 39(3), 721-736.  
399
- 400 EC-Earth Consortium (EC-Earth) (2019). EC-Earth-Consortium EC-Earth3 model output prepared for  
401 CMIP6 ScenarioMIP ssp585. Version 20211003.Earth System Grid Federation.  
402 <https://doi.org/10.22033/ESGF/CMIP6.4912>  
403
- 404 EC-Earth Consortium (EC-Earth) (2021). EC-Earth-Consortium EC-Earth-3-CC model output prepared  
405 for CMIP6 CMIP historical. Version 20211003.Earth System Grid Federation.  
406 <https://doi.org/10.22033/ESGF/CMIP6.4702>
- 407 Eyring, V., Bony, S., Meehl, G. A., Senior, C. A., Stevens, B., Stouffer, R. J., & Taylor, K. E. (2016).  
408 Overview of the Coupled Model Intercomparison Project Phase 6 (CMIP6) experimental design and  
409 organization. *Geoscientific Model Development*, 9(LLNL-JRNL-736881), 1937–1958.  
410 <https://doi.org/10.5194/gmd-9-1937-2016>
- 411 Good, Peter (2020). MOHC HadGEM3-GC31-LL model output prepared for CMIP6 ScenarioMIP  
412 ssp585. Version 20211003.Earth System Grid Federation.  
413 <https://doi.org/10.22033/ESGF/CMIP6.10901>  
414
- 415 Good, Peter; Sellar, Alistair; Tang, Yongming; Rumbold, Steve; Ellis, Rich; Kelley, Douglas; Kuhlbrodt,  
416 Till (2019). MOHC UKESM1.0-LL model output prepared for CMIP6 ScenarioMIP ssp585.  
417 Version 20211003.Earth System Grid Federation. <https://doi.org/10.22033/ESGF/CMIP6.6405>
- 418 Heuzé, C. (2021). Antarctic bottom water and North Atlantic deep water in CMIP6 models. *Ocean*  
419 *Science*, 17(1), 59–90. <https://doi.org/10.5194/os-17-59-2021>
- 420 Holt, J, P. Hyder, M. Ashworth, J. Harle, H. T. Hewitt, H. Liu, A. L. New, S. Pickles, A. Porter, E. Popova,  
421 J. I. Allen, J. Siddorn, and R. Wood (2017) Prospects for improving the representation of coastal and  
422 shelf seas in global ocean models. *Geosci. Model Dev.*, 10, 499-523.



- 423 Huang, Wenyu (2019). THU CIESM model output prepared for CMIP6 CMIP historical. Version  
424 20211003. Earth System Grid Federation. <https://doi.org/10.22033/ESGF/CMIP6.8843>  
425
- 426 Huang, Wenyu (2020). THU CIESM model output prepared for CMIP6 ScenarioMIP ssp585.  
427 Version 20211003. Earth System Grid Federation. <https://doi.org/10.22033/ESGF/CMIP6.8863>  
428
- 429 Johns, W. E., M. O. Baringer, L. M. Beal, S. A. Cunningham, T. Kanzow, H. L. Bryden, J. Hirschi, J.  
430 Marotzke, C. Meinen, B. Shaw, and R. Curry (2011) Continuous, array-based estimates of Atlantic  
431 Ocean heat transport at 26.5°N. *J. Climate*, **24**, 2429-2449.  
432
- 433 Johns, W.E., S. Elipot, D. A. Smeed, B. Moat, B. King, D. L. Volkov, and R. H. Smith (2023) Towards two  
434 decades of Atlantic Ocean mass and heat transports at 26.5 N. *Philosophical Transactions of the*  
435 *Royal Society A*, **381**(2262).  
436
- 437 Jungclaus, Johann; Bittner, Matthias; Wieners, Karl-Hermann; Wachsmann, Fabian; Schupfner,  
438 Martin; Legutke, Stephanie; Giorgetta, Marco; Reick, Christian; Gayler, Veronika; Haak, Helmut; de  
439 Vrese, Philipp; Raddatz, Thomas; Esch, Monika; Mauritsen, Thorsten; von Storch, Jin-Song; Behrens,  
440 Jörg; Brovkin, Victor; Claussen, Martin; Crueger, Traute; Fast, Irina; Fiedler, Stephanie; Hagemann,  
441 Stefan; Hohenegger, Cathy; Jahns, Thomas; Kloster, Silvia; Kinne, Stefan; Lasslop, Gitta; Kornblueh,  
442 Luis; Marotzke, Jochem; Matei, Daniela; Meraner, Katharina; Mikolajewicz, Uwe; Modali,  
443 Kameswarrao; Müller, Wolfgang; Nabel, Julia; Notz, Dirk; Peters-von Gehlen, Karsten; Pincus, Robert;  
444 Pohlmann, Holger; Pongratz, Julia; Rast, Sebastian; Schmidt, Hauke; Schnur, Reiner; Schulzweida,  
445 Uwe; Six, Katharina; Stevens, Bjorn; Voigt, Aiko; Roeckner, Erich (2019). MPI-M MPI-ESM1.2-HR  
446 model output prepared for CMIP6 CMIP historical. Version 20211003. Earth System Grid Federation.  
447 <https://doi.org/10.22033/ESGF/CMIP6.6594>  
448
- 449 Lee, J.-Y., J. Marotzke, G. Bala, L. Cao, S. Corti, J.P. Dunne, F. Engelbrecht, E. Fischer, J.C. Fyfe, C.  
450 Jones, A. Maycock, J. Mutemi, O. Ndiaye, S. Panickal, and T. Zhou, 2021: Future Global Climate:  
451 Scenario-Based Projections and Near-Term Information. In *Climate Change 2021: The Physical*  
452 *Science Basis. Contribution of Working Group I to the Sixth Assessment Report of the*  
453 *Intergovernmental Panel on Climate Change* [Masson-Delmotte, V., P. Zhai, A. Pirani, S.L. Connors, C.  
454 Péan, S. Berger, N. Caud, Y. Chen, L. Goldfarb, M.I. Gomis, M. Huang, K. Leitzell, E. Lonnoy, J.B.R.  
455 Matthews, T.K. Maycock, T. Waterfield, O. Yelekçi, R. Yu, and B. Zhou (eds.)]. Cambridge University  
456 Press, Cambridge, United Kingdom and New York, NY, USA, pp. 553–672,  
457 doi:10.1017/9781009157896.006.  
458
- 459 Levang, S. J., & Schmitt, R. W. (2020). What Causes the AMOC to Weaken in CMIP5?. *Journal of*  
460 *Climate*, **33**(4), 1535-1545.  
461
- 462 Li, G., L. Cheng, J. Zhu, K. E. Trenberth, M. E. Mann and J. P. Abraham (2020) Increasing ocean  
463 stratification over the past half-century. *Nat. Clim. Change* **10**, 1116–1123.  
464
- 465 Lovato, Tomas; Peano, Daniele (2020). CMCC CMCC-CM2-SR5 model output prepared for CMIP6  
466 CMIP historical. Version 20211003. Earth System Grid Federation.  
467 <https://doi.org/10.22033/ESGF/CMIP6.3825>  
468
- 469 Lovato, Tomas; Peano, Daniele (2020). CMCC CMCC-CM2-SR5 model output prepared for CMIP6  
470 ScenarioMIP ssp585. Version 20211003. Earth System Grid Federation.  
471 <https://doi.org/10.22033/ESGF/CMIP6.3896>  
472
- 473 Lovato, Tomas; Peano, Daniele; Butenschön, Momme (2021). CMCC CMCC-ESM2 model output  
474 prepared for CMIP6 CMIP historical. Version 20211003. Earth System Grid Federation.



- 475 <https://doi.org/10.22033/ESGF/CMIP6.13195>  
476  
477 Lovato, Tomas; Peano, Daniele; Butenschön, Momme (2021). CMCC CMCC-ESM2 model output  
478 prepared for CMIP6 ScenarioMIP ssp585. Version 20211003. Earth System Grid Federation.  
479 <https://doi.org/10.22033/ESGF/CMIP6.13259>  
480  
481 McCarthy, G. D., Smeed, D. A., Johns, W. E., Frajka-Williams, E., Moat, B. I., Rayner, D., ... & Bryden,  
482 H. L. (2015). Measuring the Atlantic meridional overturning circulation at 26 N. *Progress in*  
483 *Oceanography*, 130, 91-111.  
484  
485 Mecking, J.V. and Drijfhout, S. S. (2023). The decrease in ocean heat transport in response to global  
486 warming. *Nature Climate Change*, pp. 1-8.  
487  
488 Meinen, C. S., Johns, W. E., Moat, B. I., Smith, R. H., Johns, E. M., Rayner, D., ... & Garzoli, S. L. (2019).  
489 Structure and variability of the Antilles Current at 26.5 N. *Journal of Geophysical Research:*  
490 *Oceans*, 124(6), 3700-3723.  
491  
492 Moat B. I. et al. (2020) Pending recovery in the strength of the meridional overturning circulation at  
493 26°N. *Ocean Sci.* 16, 863–874. (doi:10.5194/os-16-863-2020).  
494  
495 Moat, B. I., Frajka-Williams, E., Smeed, D. A., Rayner, D., Johns, W. E., Baringer, M. O., et al. (2022).  
496 Atlantic meridional overturning circulation observed by the RAPID-MOCHA-WBTS (RAPID-meridional  
497 Overturning Circulation and Heatflux Array-Western Boundary Time Series) array at 26N from 2004  
498 to 2020 (v2020.2). [Dataset]. British Oceanographic Data Centre, Natural Environment Research  
499 Council. <https://doi.org/10.5285/e91b10af-6f0a-7fa7-e053-6c86abc05a09>  
500  
501 Munk, W., 1966: Abyssal recipes. *Deep-Sea Res.*, **13**, 707-730.  
502  
503 O'Neill, B. C., Tebaldi, C., Vuuren, D. P. V., Eyring, V., Friedlingstein, P., Hurtt, G., et al. (2016). The  
504 scenario model intercomparison project (ScenarioMIP) for CMIP6. *Geoscientific Model Development*,  
505 9(9), 3461–3482. <https://doi.org/10.5194/gmd-9-3461-2016>  
506  
507 Ridley, Jeff; Menary, Matthew; Kuhlbrodt, Till; Andrews, Martin; Andrews, Tim (2019). MOHC  
508 HadGEM3-GC31-LL model output prepared for CMIP6 CMIP historical. Version 20211003. Earth  
509 System Grid Federation. <https://doi.org/10.22033/ESGF/CMIP6.6109>  
510  
511 Ridley, Jeff; Menary, Matthew; Kuhlbrodt, Till; Andrews, Martin; Andrews, Tim (2019). MOHC  
512 HadGEM3-GC31-MM model output prepared for CMIP6 CMIP historical. Version 20211003. Earth  
513 System Grid Federation. <https://doi.org/10.22033/ESGF/CMIP6.6112>  
514  
515 Roberts, M. J., Jackson, L. C., Roberts, C. D., Meccia, V., Docquier, D., Koenigk, T., ... & Wu, L. (2020).  
516 Sensitivity of the Atlantic meridional overturning circulation to model resolution in CMIP6  
517 HighResMIP simulations and implications for future changes. *Journal of Advances in Modeling Earth*  
518 *Systems*, 12(8), e2019MS002014.  
519  
520 Rong, Xinyao (2019). CAMS CAMS\_CSM1.0 model output prepared for CMIP6 CMIP historical.  
521 Version 20211003. Earth System Grid Federation. <https://doi.org/10.22033/ESGF/CMIP6.9754>  
522  
523 Rong, Xinyao (2019). CAMS CAMS-CSM1.0 model output prepared for CMIP6 ScenarioMIP ssp585.  
524 Version 20211003. Earth System Grid Federation. <https://doi.org/10.22033/ESGF/CMIP6.11052>  
525  
526 Schupfner, Martin; Wieners, Karl-Hermann; Wachsmann, Fabian; Steger, Christian; Bittner, Matthias;



- 527 Jungclaus, Johann; Früh, Barbara; Pankatz, Klaus; Giorgetta, Marco; Reick, Christian; Legutke,  
528 Stephanie; Esch, Monika; Gayler, Veronika; Haak, Helmuth; de Vrese, Philipp; Raddatz, Thomas;  
529 Mauritsen, Thorsten; von Storch, Jin-Song; Behrens, Jörg; Brovkin, Victor; Claussen, Martin; Crueger,  
530 Traute; Fast, Irina; Fiedler, Stephanie; Hagemann, Stefan; Hohenegger, Cathy; Jahns, Thomas;  
531 Kloster, Silvia; Kinne, Stefan; Lasslop, Gitta; Kornbluh, Luis; Marotzke, Jochem; Matei, Daniela;  
532 Meraner, Katharina; Mikolajewicz, Uwe; Modali, Kameswarrao; Müller, Wolfgang; Nabel, Julia; Notz,  
533 Dirk; Peters-von Gehlen, Karsten; Pincus, Robert; Pohlmann, Holger; Pongratz, Julia; Rast, Sebastian;  
534 Schmidt, Hauke; Schnur, Reiner; Schulzweida, Uwe; Six, Katharina; Stevens, Bjorn; Voigt, Aiko;  
535 Roeckner, Erich (2019). DKRZ MPI-ESM1.2-HR model output prepared for CMIP6 ScenarioMIP  
536 ssp585. Version 20211003. Earth System Grid Federation.  
537 <https://doi.org/10.22033/ESGF/CMIP6.4403>  
538  
539 Seferian, Roland (2018). CNRM-CERFACS CNRM-ESM2-1 model output prepared for CMIP6 CMIP  
540 historical. Version 20211003. Earth System Grid Federation.  
541 <https://doi.org/10.22033/ESGF/CMIP6.4068>  
542  
543 Smeed, D.A., S. A. Josey, C. Beaulieu, W.E. Johns, B. I. Moat, E. Frajka-Williams, D. Rayner, C. S.  
544 Meinen, M. O. Baringer, H. L. Bryden, and G. D. McCarthy. 2018. The North Atlantic Ocean is in a  
545 state of reduced overturning, *Geophysical Research Letters*, 45,  
546 <https://doi.org/10.1002/2017GL076350>.  
547  
548 Song, Zhenya; Qiao, Fangli; Bao, Ying; Shu, Qi; Song, Yajuan; Yang, Xiaodan (2019). FIO-QLNM FIO-  
549 ESM2.0 model output prepared for CMIP6 CMIP historical. Version 20211003. Earth System Grid  
550 Federation. <https://doi.org/10.22033/ESGF/CMIP6.9199>  
551  
552 Song, Zhenya; Qiao, Fangli; Bao, Ying; Shu, Qi; Song, Yajuan; Yang, Xiaodan (2019). FIO-QLNM FIO-  
553 ESM2.0 model output prepared for CMIP6 ScenarioMIP ssp585. Version 20211003. Earth System Grid  
554 Federation. <https://doi.org/10.22033/ESGF/CMIP6.9214>  
555  
556 Stommel, H. (1948). The westward intensification of wind-driven ocean currents. *Eos, Transactions*  
557 *American Geophysical Union*, 29(2), 202-206.  
558  
559 Swart, Neil Cameron; Cole, Jason N.S.; Kharin, Viatcheslav V.; Lazare, Mike; Scinocca, John F.; Gillett,  
560 Nathan P.; Anstey, James; Arora, Vivek; Christian, James R.; Jiao, Yanjun; Lee, Warren G.; Majaess,  
561 Fouad; Saenko, Oleg A.; Seiler, Christian; Seinen, Clint; Shao, Andrew; Solheim, Larry; von Salzen,  
562 Knut; Yang, Duo; Winter, Barbara; Sigmond, Michael (2019). CCCma CanESM5 model output  
563 prepared for CMIP6 CMIP historical. Version 20211003. Earth System Grid Federation.  
564 <https://doi.org/10.22033/ESGF/CMIP6.3610>  
565  
566 Swart, Neil Cameron; Cole, Jason N.S.; Kharin, Viatcheslav V.; Lazare, Mike; Scinocca, John F.; Gillett,  
567 Nathan P.; Anstey, James; Arora, Vivek; Christian, James R.; Jiao, Yanjun; Lee, Warren G.; Majaess,  
568 Fouad; Saenko, Oleg A.; Seiler, Christian; Seinen, Clint; Shao, Andrew; Solheim, Larry; von Salzen,  
569 Knut; Yang, Duo; Winter, Barbara; Sigmond, Michael (2019). CCCma CanESM5 model output  
570 prepared for CMIP6 ScenarioMIP ssp585. Version 20211003. Earth System Grid Federation.  
571 <https://doi.org/10.22033/ESGF/CMIP6.3696>  
572  
573 Tang, Yongming; Rumbold, Steve; Ellis, Rich; Kelley, Douglas; Mulcahy, Jane; Sellar, Alistair; Walton,  
574 Jeremy; Jones, Colin (2019). MOHC UKESM1.0-LL model output prepared for CMIP6 CMIP  
575 historical. Version 20211003. Earth System Grid Federation.  
576 <https://doi.org/10.22033/ESGF/CMIP6.6113>



- 577 Toggweiler, J. R., & Samuels, B. (1998). On the ocean's large-scale circulation near the limit of no  
578 vertical mixing. *Journal of Physical Oceanography*, 28(9), 1832–1852. [https://doi.org/10.1175/1520-](https://doi.org/10.1175/1520-0485(1998)028)  
579 [0485\(1998\)028](https://doi.org/10.1175/1520-0485(1998)028)
- 580 Voltaire, Aurore (2019). CNRM-CERFACS CNRM-CM6-1-HR model output prepared for CMIP6 CMIP  
581 historical. Version 20211003. Earth System Grid Federation.  
582 <https://doi.org/10.22033/ESGF/CMIP6.4067>  
583
- 584 Voltaire, Aurore (2019). CNRM-CERFACS CNRM-CM6-1-HR model output prepared for CMIP6  
585 ScenarioMIP ssp585. Version 20211003. Earth System Grid Federation.  
586 <https://doi.org/10.22033/ESGF/CMIP6.4225>  
587
- 588 Weijer, W., Cheng, W., Garuba, O. A., Hu, A., & Nadiga, B. T. (2020). CMIP6 models predict significant  
589 21st century decline of the Atlantic Meridional Overturning Circulation. *Geophysical Research*  
590 *Letters*, 47(12), e2019GL086075.  
591
- 592 Wieners, Karl-Hermann; Giorgetta, Marco; Jungclaus, Johann; Reick, Christian; Esch, Monika; Bittner,  
593 Matthias; Legutke, Stephanie; Schupfner, Martin; Wachsmann, Fabian; Gayler, Veronika; Haak,  
594 Helmuth; de Vrese, Philipp; Raddatz, Thomas; Mauritsen, Thorsten; von Storch, Jin-Song; Behrens,  
595 Jörg; Brovkin, Victor; Claussen, Martin; Crueger, Traute; Fast, Irina; Fiedler, Stephanie; Hagemann,  
596 Stefan; Hohenegger, Cathy; Jahns, Thomas; Kloster, Silvia; Kinne, Stefan; Lasslop, Gitta; Kornblueh,  
597 Luis; Marotzke, Jochem; Matei, Daniela; Meraner, Katharina; Mikolajewicz, Uwe; Modali,  
598 Kameswarrao; Müller, Wolfgang; Nabel, Julia; Notz, Dirk; Peters-von Gehlen, Karsten; Pincus, Robert;  
599 Pohlmann, Holger; Pongratz, Julia; Rast, Sebastian; Schmidt, Hauke; Schnur, Reiner; Schulzweida,  
600 Uwe; Six, Katharina; Stevens, Bjorn; Voigt, Aiko; Roeckner, Erich (2019). MPI-M MPI-ESM1.2-LR  
601 model output prepared for CMIP6 CMIP historical. Version 20211003. Earth System Grid  
602 Federation. <https://doi.org/10.22033/ESGF/CMIP6.6595>  
603
- 604 Wieners, Karl-Hermann; Giorgetta, Marco; Jungclaus, Johann; Reick, Christian; Esch, Monika; Bittner,  
605 Matthias; Gayler, Veronika; Haak, Helmuth; de Vrese, Philipp; Raddatz, Thomas; Mauritsen,  
606 Thorsten; von Storch, Jin-Song; Behrens, Jörg; Brovkin, Victor; Claussen, Martin; Crueger, Traute;  
607 Fast, Irina; Fiedler, Stephanie; Hagemann, Stefan; Hohenegger, Cathy; Jahns, Thomas; Kloster, Silvia;  
608 Kinne, Stefan; Lasslop, Gitta; Kornblueh, Luis; Marotzke, Jochem; Matei, Daniela; Meraner, Katharina;  
609 Mikolajewicz, Uwe; Modali, Kameswarrao; Müller, Wolfgang; Nabel, Julia; Notz, Dirk; Peters-von  
610 Gehlen, Karsten; Pincus, Robert; Pohlmann, Holger; Pongratz, Julia; Rast, Sebastian; Schmidt, Hauke;  
611 Schnur, Reiner; Schulzweida, Uwe; Six, Katharina; Stevens, Bjorn; Voigt, Aiko; Roeckner,  
612 Erich (2019). MPI-M MPI-ESM1.2-LR model output prepared for CMIP6 ScenarioMIP  
613 ssp585. Version 20211003. Earth System Grid Federation.  
614 <https://doi.org/10.22033/ESGF/CMIP6.6705>  
615
- 616 Yan, X., Zhang, R., & Knutson, T. R. (2018). Underestimated AMOC variability and implications for  
617 AMV and predictability in CMIP models. *Geophysical Research Letters*, 45(9), 4319–4328.  
618
- 619 Yukimoto, Seiji; Koshiro, Tsuyoshi; Kawai, Hideaki; Oshima, Naga; Yoshida, Kohei; Urakawa, Shogo;  
620 Tsujino, Hiroaki; Deushi, Makoto; Tanaka, Taichu; Hosaka, Masahiro; Yoshimura, Hiromasa; Shindo,  
621 Eiki; Mizuta, Ryo; Ishii, Masayoshi; Obata, Atsushi; Adachi, Yukimasa (2019). MRI MRI-ESM2.0 model  
622 output prepared for CMIP6 CMIP historical. Version 20211003. Earth System Grid  
623 Federation. <https://doi.org/10.22033/ESGF/CMIP6.6842>  
624
- 625 Yukimoto, Seiji; Koshiro, Tsuyoshi; Kawai, Hideaki; Oshima, Naga; Yoshida, Kohei; Urakawa, Shogo;  
626 Tsujino, Hiroaki; Deushi, Makoto; Tanaka, Taichu; Hosaka, Masahiro; Yoshimura, Hiromasa; Shindo,  
627 Eiki; Mizuta, Ryo; Ishii, Masayoshi; Obata, Atsushi; Adachi, Yukimasa (2019). MRI MRI-ESM2.0 model



628 output prepared for CMIP6 ScenarioMIP ssp585. Version 20211003. Earth System Grid Federation.  
629 <https://doi.org/10.22033/ESGF/CMIP6.6929>  
630  
631 Zhao, J., & Johns, W. (2014). Wind-forced interannual variability of the Atlantic Meridional  
632 Overturning Circulation at 26.5 N. *Journal of Geophysical Research: Oceans*, 119(4), 2403-2419.